DRAFT VERSION DECEMBER 22, 2016
Typeset using LaTeX **twocolumn** style in AASTeX61

arXiv:1612.06884v1 [physics.plasm-ph] 19 Dec 2016

DETERMINATION OF PLASMA SCREENING EFFECTS FOR THERMONUCLEAR REACTIONS IN LASER-GENERATED PLASMAS

YUANBIN WU[1] AND ADRIANA PÁLFFY[1]

[1]*Max-Planck-Institut für Kernphysik, Saupfercheckweg 1, D-69117 Heidelberg, Germany*

ABSTRACT

Due to screening effects, nuclear reactions in astrophysical plasmas may behave differently than in the laboratory. The possibility to determine the magnitude of these screening effects in colliding laser-generated plasmas is investigated theoretically, having as starting point a proposed experimental setup with two laser beams at the Extreme Light Infrastructure facility. A laser pulse interacting on a solid target produces a plasma through the Target Normal Sheath Acceleration scheme, and this rapidly streaming plasma (ion flow) impacts on a secondary plasma created by the interaction of a second laser pulse on a gas jet target. We model here this scenario and calculate the reaction events for the astrophysically relevant reaction ^{13}C(^{4}He,n)^{16}O. We find that it should be experimentally possible to determine the plasma screening enhancement factor for fusion reactions by detecting the difference in reaction events between two scenarios of ion flow interacting with the plasma target and a simple gas target. This provides a way to evaluate nuclear reaction cross-sections in stellar environments and can significantly advance the field of nuclear astrophysics.

Keywords: thermonuclear reactions, plasma screening, Extreme Light Infrastructure, nuclear astrophysics

yuanbin.wu@mpi-hd.mpg.de

Palffy@mpi-hd.mpg.de

1. INTRODUCTION

In astrophysical environments, matter is usually found in the state of plasma. Stars are made of dense plasmas, and the intergalactic, interstellar, as well as the interplanetary medium consist mainly of diffuse plasmas. Thus, plasma plays a very important role in the universe. The properties of nuclear matter, such as reaction mechanisms and life times, may drastically differ in the plasma environment from the ones in conventional laboratory environments. In this context, the role of charge screening is a crucial aspects.

Charge screening enhances the nuclear cross sections by reducing the Coulomb barrier that reacting ions must overcome. There are basically two kinds of charge screening effects for the fusion of two positively charged nuclei (Adelberger et al. 2011). One is the electron screening applied to the laboratory reactions which generally involve target nuclei bound in neutral atoms and molecules (Assenbaum et al. 1987). The atomic (or molecular) electron cloud surrounding the target nucleus acts as a screening potential (Assenbaum et al. 1987). This screening effect becomes important when the projectile energy is very low (Adelberger et al. 2011; Assenbaum et al. 1987). The second type of screening effect is the plasma (electrostatic) screening (Salpeter 1954; Keller 1953; Salpeter & Van Horn 1969; Graboske et al. 1973; Dzitko et al. 1995; Gruzinov & Bahcall 1998) applied to the stellar (thermonuclear) reactions that happen in plasma environments in which most atoms are ionized. In plasmas, long-range electric fields are screened down by the dynamic flow of particles moving in response to electric fields. It is necessary to take into account the effects of this screening on the rate of thermonuclear reactions in stars (Adelberger et al. 2011).

In the past decades, many experiments that test the first type of electron screening in laboratory reactions with targets in the form of neutral atoms or molecules have been performed (Adelberger et al. 2011; Assenbaum et al. 1987; Rolfs & Somorjai 1995; Rolfs 2001; Engstler et al. 1988, 1992; Greife et al. 1995; Aliotta et al. 2001). These experiments are not only important for the understanding of electron screening, but also for extracting bare cross sections which are needed as inputs for stellar reactions (Adelberger et al. 2011). In contrast with the case of laboratory screening, the plasma screening for stellar reactions is so far lacking experimental tests (Adelberger et al. 2011). Determining the appropriate experimental conditions that allow to evaluate the nuclear reactions in stellar environments could significantly contribute to the field of nuclear astrophysics. The study of direct measurements of reactions in laser-generated plasmas provides this opportunity (Roth et al. 2015) [we point out here that appropriate experimental conditions for the study of atomic processes are also important for the understanding of the astrophysical observation results (Bernitt et al. 2012; Oreshkina et al. 2014); however it is out of the scope of the present work]. We note that the use of colliding laser-generated plasma plumes for nuclear physics studies was proposed few years ago (Mascali et al. 2010) and was already experimentally demonstrated for the neutronless $p+^{11}$Be fusion reaction (Labaune et al. 2013).

At the upcoming Nuclear Pillar of the Extreme Light Infrastructure (ELI-NP) facility in construction in Romania, two high-power lasers working in parallel will be available (Roth et al. 2015). Each laser pulse can reach a peak power up to 10 PW, with the typical pulse duration of ~ 25 fs. At this facility, an experimental setup in which two laser beams generate two colliding plasmas is envisaged in the Techical Design Report (TDR) (Roth et al. 2015) [see also the published version thereof (Negoita et al. 2016)]. This will give the opportunity to investigate nuclear reactions under plasma conditions. The target configuration of the proposed experimental setup is shown in Fig. 1. A laser pulse interacting on a solid-state target produces a plasma through the Target Normal Sheath Acceleration (TNSA) mechanism [see (Macchi et al. 2013) and references therein], and this rapidly streaming plasma (ion flow) interacts on a secondary plasma created by the interaction of a second laser pulse on a gas jet target. A high granularity SiC charged-particle detector and a neutron time-of-flight detector, not shown here in Fig. 1, are placed after the target in the forward direction of the ion flow from TNSA, covering a quite large angle of the outgoing nuclear reaction products (Roth et al. 2015). This setup would allow the study of direct measurements of nuclear reaction rates in plasma environments.

In this paper, we address this scenario from the theoretical side. We apply an isothermal, fluid model (Mora 2003; Fuchs et al. 2006) to describe the TNSA mechanism in the laser-target interaction. With the ion spectrum obtained from this model, we study the nuclear fusion reactions in the interaction of the rapidly streaming plasma (ion flow) on the secondary plasma. As the first case of study, we analyze the reaction ^{13}C(^{4}He,n)^{16}O, which is one of the important helium burning processes as well as one of the main neutron sources for the s-process (De Loore & Doom 1992; Gallino et al. 1998; Heil et al. 2008). We consider the interaction of the TNSA-accelerated ions with both a plasma target and with a gas target. Our results show that a direct comparison of the neutron events considering the two types of targets should provide experimental access to the screening effects for the colliding plasma scenario. This would be the first time when experiments with laser-created plasmas in the laboratory could give insight on screening effects for thermonuclear reactions in astrophysical plasmas. We discuss the parameters that allow the determination of the plasma screening effect.

The paper is organized as follows. In Sec. 2, we present the fluid model for the TNSA scheme. We describe the plasma screening enhancement for fusion reactions of two positively charged nuclei in Sec. 3. Our results and discussion on the reaction ^{13}C(^{4}He,n)^{16}O follow in Sec. 4. We finally summarize and conclude in Sec. 5. In Sec. 2, SI units with $k_B = 1$ are adopted, unless for some quantities the units are explicitely given. In Sec. 3, the Lorentz-Heaviside natural units $\hbar = c = \varepsilon_0 = \mu_0 = k_b = 1$ are adopted.

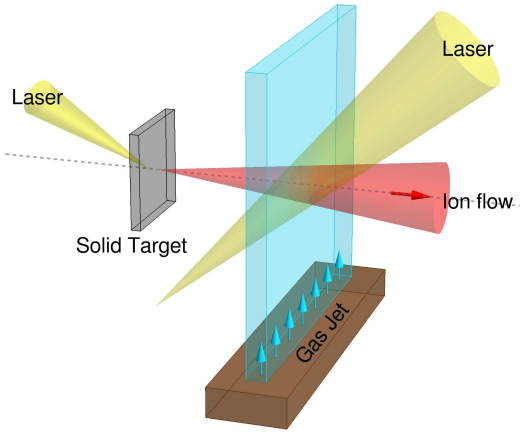

Figure 1. The proposed experimental setup for nuclear reactions in laser-generated plasmas at ELI-NP for the ^{13}C(^{4}He,n)^{16}O reaction. The carbon ions are expelled and accelerated from the first solid target via the TNSA mechanism. They meet the gas jet or plasma He target and the nuclear reaction products are detected in the forward direction. A similar figure is illustrated in Ref. Roth et al. (2015).

2. TNSA MODEL

In this section, we introduce a model to describe the Target Normal Sheath Acceleration (TNSA) scheme in the laser-target interaction, based on the fluid model of plasma expansion into a vacuum studied in Ref. Mora (2003). The model in Ref. Mora (2003) is an isothermal, fluid model, in which the charge separation effects in the collisionless plasma expansion were studied. In this model, at time $t = 0$, the plasma is assumed to occupy the half-space $x < 0$. The ions are cold and initially at rest with density $n_i = n_{i0}$ for $x < 0$ and $n_i = 0$ for $x > 0$ with a sharp boundary. The electron density n_e is continuous and corresponds to a Boltzmann distribution with the electron temperature T_e. In addition, one also has $\Phi(-\infty) = 0$ and $n_{e0} = Z_i n_{i0}$, with Z_i being the ion charge state, n_{e0} the electron density in the unperturbed plasma, and Φ the electrostatic potential. Assuming quasi-neutrality in the expanding plasma, a self-similar expansion can be found for $x + c_s t > 0$ (Mora 2003), i.e., $n_e = Z_i n_i = n_{e0} \exp[-x/(c_s t) - 1]$ and $v_i = c_s + x/t$, where c_s is the ion sound speed, $c_s = \sqrt{Z_i T_e/m_i}$, v_i is the ion velocity, and m_i is the ion mass. Based on the self-similar expansion and numerical solutions of the fluid model, Mora obtained the ion energy spectrum and the maximum ion energy (Mora 2003).

Following the procedure described in Ref. Fuchs et al. (2006), we can apply this fluid model of plasma expansion to study the TNSA scheme in the laser-target interaction. Since this occurs in most experiments, Ref. Fuchs et al. (2006) considers a preformed plasma (preplasma) is present in front of the target owing to long-duration, low-level laser energy (prepulse) reaching the target before the main pulse. The electrons are accelerated following the irradiation by the main pulse. The density n_{e0} can be estimated by considering that the electrons accelerated at the target front surface are ballistically sprayed into the target. As the electrons are accelerated over the laser pulse duration and spread over the surface of the sheath S_{sheath}, we have $n_{e0} = N_e/(c\tau_{laser} S_{sheath})$, where N_e is the total number of electrons accelerated into the target, and τ_{laser} is the laser pulse duration. The surface of the sheath S_{sheath} is given by

$$S_{sheath} = \pi(r_0 + d_t \tan\theta)^2, \tag{1}$$

depending on the half-angle divergence ($\theta \sim 25^o$) of the hot electron inside the target (Fuchs et al. 2003, 2006), the target thickness d_t and the initial radius r_0 of the zone over which the electrons are accelerated at the target front surface, i.e., the laser spot [r_0 is given by the half of the full width at half maximum (FWHM)].

According to the model in Ref. Mora (2003), the maximum (cutoff) energy that can be gained by the accelerated ions is (Fuchs et al. 2006)

$$\mathbb{E}_{max} = 2\mathscr{E}_0 \left[\ln\left(t_p + \sqrt{t_p^2 + 1}\right)\right]^2, \tag{2}$$

where $t_p = \omega_{pi} t_{acc}/\sqrt{2\mathrm{Exp}}$ is the normalized acceleration time, and $\mathscr{E}_0 = Z_i T_e$. Furthermore, ω_{pi} is the ion plasma frequency, $\omega_{pi} = \sqrt{n_{e0} Z_i e^2/(m_i \varepsilon_0)}$, and t_{acc} is the effective acceleration time. As shown in Ref. Fuchs et al. (2006), $t_{acc} \sim 1.3\tau_{laser}$ matches well with experimental results. The number of accelerated ions per unit energy is given by (Mora 2003; Fuchs et al. 2006)

$$\frac{dN}{d\mathbb{E}} = \frac{n_{i0} c_s t_{acc} S_{steath}}{\sqrt{2\mathbb{E}\mathscr{E}_0}} \exp\left(-\sqrt{2\mathbb{E}/\mathscr{E}_0}\right). \tag{3}$$

In order to obtain the cutoff energy and the energy spectrum of the ions, the ion and electron densities and the electron temperature must be known. The ponderomotive scaling (Wilks et al. 1992; Malka & Miquel 1996; Fuchs et al. 2006) is adopted for the electron temperature,

$$T_e = m_e c^2 \left[\sqrt{1 + I\lambda_{\mu m}^2/1.37 \times 10^{18}} - 1\right], \tag{4}$$

where m_e is the electron mass, I is the laser intensity in W/cm^2, and $\lambda_{\mu m}$ is the laser wavelength in micrometers. As

shown in Ref. Fuchs et al. (2006), the total number of electrons accelerated into the target is

$$N_{\rm e} = f_{\rm abs} E_{\rm laser}/T_{\rm e}, \tag{5}$$

where $E_{\rm laser}$ is the laser energy and $f_{\rm abs}$ is the fraction of laser light that is absorbed into the preplasma as fast electrons. According to available experimental results, the empirical fraction $f_{\rm abs}$ can be given as (Fuchs et al. 2006)

$$f_{\rm abs} = 1.2\times10^{-15} I^{0.74} \tag{6}$$

with a maximum of 0.5.

We now turn to the charge state of the ions in the plasma. As shown in Ref. Hegelich et al. (2002), with the strong space-charge field created at the rear surface of the target in TNSA, field ionization by barrier suppression is the dominant ionization mechanism at the rear of the target. The $q+$ ionic state will be created as soon as the electric filed is above the threshold (Hegelich et al. 2002)

$$E_q^{\rm thresh} = U_q^2 \varepsilon_0 \pi / qe, \tag{7}$$

where U_q is the ionization potential in eV. As a first approximation, we assume $Z_{\rm i}$ as the charge state that can be reached under the initial electric field at the ion front predicted by the fluid model (Mora 2003) discussed here,

$$E_{\rm front,0} = \sqrt{2/{\rm Exp}}(n_{\rm e0} T_{\rm e}/\varepsilon_0)^{1/2}. \tag{8}$$

For the case of ^{13}C under consideration, we adopt the values of U_q and $E_q^{\rm thresh}$ used in Ref. Hegelich et al. (2002). These values are also shown in Table 1.

q	U_q [eV]	$E_q^{\rm thresh}$ [V/m]
1	11.2	2.2×10^{10}
2	24.4	5.2×10^{10}
3	47.9	1.3×10^{11}
4	64.5	1.8×10^{11}
5	392	5.3×10^{12}
6	490	7.0×10^{12}

Table 1. The ionization potential U_q and threshold $E_q^{\rm thresh}$ of the electric field for the creation of the $q+$ charged state state of carbon. These values are adopted from Ref. Hegelich et al. (2002).

3. NUCLEAR REACTIONS IN PLASMAS

The cross section for the fusion of two positively charged nuclei is often written as [see, e.g., (Assenbaum et al. 1987; Atzeni & Meyer-ter Vehn 2004; Raiola et al. 2002)]

$$\sigma(\mathbb{E}_{\rm c}) = \frac{S(\mathbb{E}_{\rm c})}{\mathbb{E}_{\rm c}} \exp(-2\pi\eta), \tag{9}$$

where $\mathbb{E}_{\rm c}$ is the center-of-mass (c.m.) energy, $S(\mathbb{E}_{\rm c})$ is the astrophysical factor, and η is the Sommerfeld parameter, $\eta = Z_1 Z_2 \alpha \sqrt{m_{\rm r}/(2\mathbb{E}_{\rm c})}$ with α being the fine-structure constant. Here, Z_1 and Z_2 are the charge numbers of the interacting nuclei and $m_{\rm r}$ is their reduced mass, $m_{\rm r} = m_1 m_2/(m_1+m_2)$, where m_1 and m_2 are the masses of the nuclei. The cross section provided in Eq. (9) assumes that the Coulomb potential of the interacting nuclei is that resulting from bare nuclei. However, this picture of nuclear reactions could be drastically affected inside plasmas, owing to the charge screening effects. According to the classical theory of plasmas, in weakly coupled plasmas, i.e., plasmas in which the Coulomb interaction energy between the nucleus and the nearest few electrons and nuclei is small compared with the thermal energy T, each particle only feels the effect of the particles at a distance smaller than the Debye length while on longer scales the plasma is quasi-neutral (Atzeni & Meyer-ter Vehn 2004). The nuclear reaction rate in such a plasma is therefore enhanced by a factor (Salpeter 1954; Gruzinov & Bahcall 1998)

$$g_{\rm scr} = \exp\left(\frac{Z_1 Z_2 \alpha}{T\lambda_{\rm D}}\right), \tag{10}$$

where $\lambda_{\rm D}$ is the Debye length,

$$\frac{1}{\lambda_{\rm D}^2} = 4\pi n \alpha \zeta^2 / T, \tag{11}$$

with

$$\zeta = \left[\Sigma_i X_i \frac{Z_i^2}{A_i} + \left(\frac{f'}{f}\right)\Sigma_i X_i \frac{Z_i}{A_i}\right]^{1/2}, \tag{12}$$

and n being the baryon number density. Here, X_i, Z_i, and A_i are the mass fraction, the nuclear charge, and the atomic weight of ions of type i, respectively. The ratio f'/f accounts for the electron degeneracy (Salpeter 1954), which for the plasmas under consideration $f'/f \simeq 1$. The detailed description of the term f'/f can be found in Ref. Salpeter (1954). It is important to notice here that the Salpeter formula (10) is valid under the assumption (Salpeter 1954)

$$\mathscr{I}_{\rm z} = \left(\frac{Z\alpha}{2a_{0\rm z}}\right) T^{-1} \ll 1, \tag{13}$$

where $\mathscr{I}_{\rm z}$ stands for the ratio of the ionization potential of a K-shell electron in a hydrogen-like atom of charge Z to the mean thermal energy and $a_{0\rm z}$ is the Bohr radius for such an atom. Under this assumption, all atoms are completely ionized.

The averaged reactivity for the fusion of two positively charged nuclei in plasmas can be written as (Atzeni & Meyer-ter Vehn 2004; Salpeter 1954; Gruzinov & Bahcall 1998)

$$<\sigma v>_{\rm scr} = g_{\rm scr} <\sigma v>, \tag{14}$$

where $<\sigma v>$ is the averaged reactivity neglecting screening.

The expression (10) is valid for the weak-screening case. In astrophysical environments, in addition to the weak-screening regime, it is also possible to reach the intermediate-screening and the strong-screening regimes (Salpeter 1954; Salpeter & Van Horn 1969; Graboske et al. 1973; Dzitko et al. 1995; Gruzinov & Bahcall 1998) when going to more extreme conditions. However, in the plasmas under consideration here which are produced by an intense optical laser interacting on a gas jet target, the density is typically lower than 10^{21} cm^{-3} and the temperature reaches values between ~ 100 eV and a few keV. For these parameters, the weak screening effect applies and we focus in the following on this regime.

4. RESULTS AND DISCUSSION

In this section, we present our numerical results and discussion for the reaction ^{13}C(^{4}He,n)^{16}O in ^{4}He plasmas. As shown in the Salpeter formula (10), high-density plasmas are preferred in order to have a significantly large screening enhancement. With already available technology, gas jets with density of several times of 10^{20} cm^{-3} can be obtained [see, e.g., Ref. Schmid & Veisz (2012)]. Therefore, in the present work we focus on the density range between 10^{20} cm^{-3} and 10^{21} cm^{-3} for ^{4}He. The plasma target is then created by a second laser interacting with the gas jet, as illustrated in Fig. 1. The requirements on this laser are less stringent than the ones for the first laser responsible for TNSA; in particular, a large power and high-energy pulse would be advantageous for a large focal spot and stable operation over a longer pulse duration. However, already intensities of 10^{14} W/cm^2 are sufficient to create the target plasma. We note that some rough numerical simulations for nuclear reactions in the gas jet target have been presented in the original ELI-NP TDR (Roth et al. 2015), however focusing mostly on low gas jet densities ($\sim 10^{18}$ cm^{-3}) and the low-energy part of the reactions. In this work, we go beyond that to address the plasma screening effects in fusion reactions.

Figure 2 shows the enhancement factor $g_{\rm scr}$ as a function of the temperature T for the reaction ^{13}C(^{4}He,n)^{16}O in ^{4}He plasmas predicted by the formula (10); results for selected Helium densities are shown in Fig. 2(a) and results for different carbon charge states are shown in Fig. 2(b). The plots show that the enhancement factor approaches unity for high plasma temperatures. The screening effects are quite small for temperatures $T \sim 1$ keV in the plasmas under consideration. When decreasing the plasma temperature to $T \sim 100$ eV, the enhancement factor $g_{\rm scr}$ becomes significantly large, as it is comparable with values in astrophysical scenarios [see, e.g., Refs. Salpeter (1954); Dzitko et al. (1995); Gruzinov & Bahcall (1998)]. Therefore, in the following, we focus on the cases for ^{4}He plasmas with temperature $T = 100$ eV.

Turning to the ^{13}C ions produced in the TNSA scenario, we show in Fig. 3 two examples of ion spectra predicted by the TNSA model described in Sec. 2. In these two examples, a ^{13}C target thickness of 5 μm is considered. We first consider the case of a laser of peak intensity $I = 10^{20}$ W/cm^2, peak power $P = 10$ PW and pulse duration $\tau_{\rm laser} = 25$ fs (FWHM) interacting with the target (we denote this case as case A). The space-charge field created at the rear surface of the target can reach a value higher than 10^{13} V/m. Therefore, ^{13}C ions with the charge state 6+ can be produced. As a second case we consider the interaction with a laser of peak intensity $I = 10^{19}$ W/cm^2, peak power $P = 1$ PW and pulse duration $\tau_{\rm laser} = 250$ fs (FWHM) (we denote this case as case B). Now only a lower space-charge field can be created. Therefore, only up to C^{4+} can be produced in this case. We adopt in this work a wavelength of 800 nm for the laser, which is the same as the one of the two ELI-NP lasers (Roth et al. 2015).

In Fig. 3 it is shown that for case A, a larger number of high-energy ions can be obtained than in case B, although they have similar values for the low energy part. As shown in the ponderomotive scaling (4), the electron temperature is higher for the case of the high-intensity laser. Therefore, the exponential term in Eq. (3) decreases slower for the high-intensity laser, compared to the increasing of the ion energy. Put in other words, since the space-charge field created at the rear surface of the target is higher for case A, it is obvious that this configuration can accelerate more ions to high energy.

Now we turn to the calculation of neutron events for the reaction ^{13}C(^{4}He,n)^{16}O in the envisaged experimental setup, considering the ion spectra calculated by the TNSA model described in Sec. 2. In order to do this, knowledge of the nuclear cross section for the reaction ^{13}C(^{4}He,n)^{16}O is also necessary. A combination of experimental results and a fit of the data for the reaction ^{13}C(^{4}He,n)^{16}O has been shown in Ref. Xu et al. (2013) (NACRE II). We adopt here as an approximation the fit of the $S(\mathbb{E}_{\rm c})$ in Ref. Xu et al. (2013) for the low energy part ($\mathbb{E}_{\rm c} < 0.97$ MeV), and the cross-section data form Ref. Harissopulos et al. (2005) for the high energy part ($\mathbb{E}_{\rm c} > 0.97$ MeV), respectively.

Taking into account that the density of ions from TNSA is normally much lower than the density of the secondary target under consideration, the influence of the fast ions from TNSA on the secondary target is expected to be negligible. The reaction events per laser pulse per unit energy of the incident fast ions are then given as

$$\frac{d\mathbb{N}}{d\mathbb{E}} = \frac{dN}{d\mathbb{E}} g_{\rm scr} <\sigma(\mathbb{E}_{\rm c})> n_{\rm s} d, \qquad (15)$$

for fusion reactions in a secondary plasma target with the (secondary target) ion number density $n_{\rm s}$ of and the thickness d. Furthermore, $<\sigma(\mathbb{E}_{\rm c})>$ stands for the averaged cross section under the Maxwellian distribution of the plasma target. For the sake of self-consistency and simplicity, in numerical

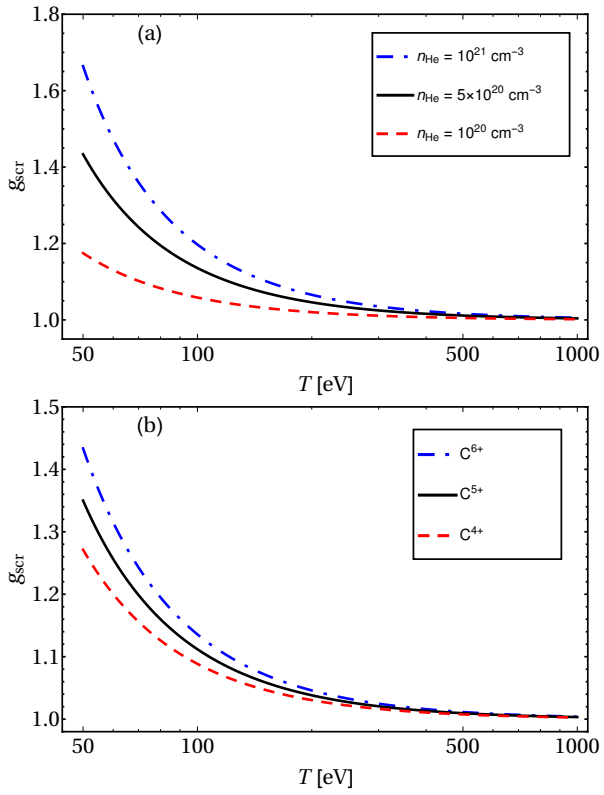

Figure 2. The enhancement factor $g_{\rm scr}$ as a function of the temperature T for the reaction ^{13}C(^{4}He,n)^{16}O in ^{4}He plasmas for (a) the cases of C^{6+} with different helium densities and (b) for the cases of $n_{\rm He} = 5\times10^{20}$ cm^{-3} with different carbon charge states.

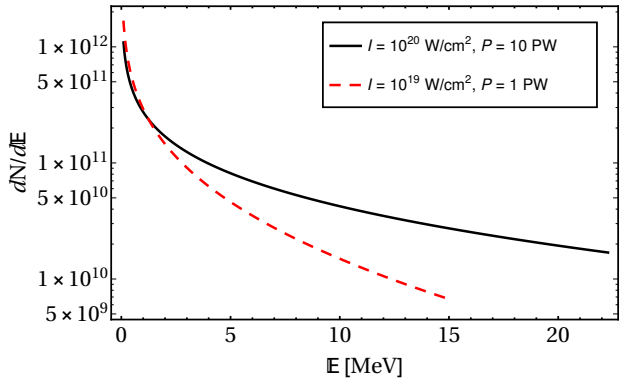

Figure 3. The number of TNSA-accelerated ^{13}C ions per unit energy. The thickness of the ^{13}C target is 5 μm. Solid black line: laser parameters corresponding to case A described in text. In this case, the charge state of the ^{13}C ions is 6+. Dashed red curve: laser parameters corresponding to case B described in text. In this case, the charge state of the ^{13}C ions is 4+.

calculations, $<\sigma(\mathbb{E}_{\rm c})>$ is obtained from a one dimensional (1-D) system, since also the model adopted here for TNSA is a 1-D model. In addition, we also show here the reaction events per laser pulse per unit energy of the incident fast ions for fusion reactions in a secondary gas target,

$$\frac{d\mathbb{N}}{d\mathbb{E}} = \frac{dN}{d\mathbb{E}}\sigma(\mathbb{E}_{\rm c})n_{\rm s}d. \qquad (16)$$

It is worth mentioning here that the reaction events Eqs. (15) and (16) are given under the assumption that the secondary target is a thin target such that the stopping of the fast ions passing through the target is negligible. Applying now the expressions above to the reaction ^{13}C(^{4}He,n)^{16}O in the considered experimental setup, $d\mathbb{N}/d\mathbb{E}$ of Eqs. (15) and (16) give the neutron events per laser pulse per unit energy of the incident fast ions, and the density $n_{\rm s}$ becomes the ^{4}He density $n_{\rm He}$.

We show in Fig. 4 the neutron spectra for the reaction ^{13}C(^{4}He,n)^{16}O in ^{4}He plasmas with temperatures $T = 100$ eV and $T = 1$ keV. For the TNSA part, we adopt the same target and laser parameters as in the case A of Fig. 3. The ^{4}He plasma density $n_{\rm He}$ is 5×10^{20} cm^{-3} and the thickness of the plasma is 20 μm. We can learn from Fig. 4 that when the ^{13}C ion energy $\mathbb{E} \lesssim 4$ MeV, the number of neutron events is very small. This is mainly due to the small cross section of the reaction for $\mathbb{E}_{\rm c} \lesssim 1$ MeV. Figure 4 also shows a quite strong averaging effect due to the plasma for the case of $T = 1$ keV. The feature of detailed resonances in the cross section [see (Xu et al. 2013)] is washed out by the plasma at the higher temperature, and the neutron spectrum has thus a smoother appearance. In contrast, for the case of $T = 100$ eV shown in Fig. 4(a), the neutron spectrum clearly follows the detailed feature of the cross section.

Integrating Eqs. (15) and (16), we obtain the total number $\mathbb{N}$ of neutron events per laser pulse for the reaction under investigation. The results of total number $\mathbb{N}$ of neutron events per laser pulse are shown in Table 2, in the cases of ^{4}He plasma with density $n_{\rm He} = 5\times10^{20}$ cm^{-3}, thickness 20 μm, and temperature 100 eV. Several laser parameter sets and target thicknesses for TNSA are adopted in Table 2. For the sake of comparison, we also show in Table 2 the total number of neutron events for the cases of a ^{4}He gas target. The number of neutron events in the case of the carbon ions interacting with the plasma is significantly larger than the one interacting with the gas target; in particular the differences are larger than 10% for the cases of C^{6+}. These differences are mainly coming from the screening enhancement, since the energy contribution from the plasma to the reaction is negligible for the case of $T = 100$ eV [see also Fig. 4(a)]. The detection of these differences could determine for the first time experimentally the screening enhancement factor.

Furthermore, we show in Table 3 the total number of neutron events per laser pulse for selected ^{4}He densities. Here, we adopt the same target and laser parameters as in case A of Fig. 3 for the TNSA part. As expected, the difference between the two scenarios of fast ions interacting with the

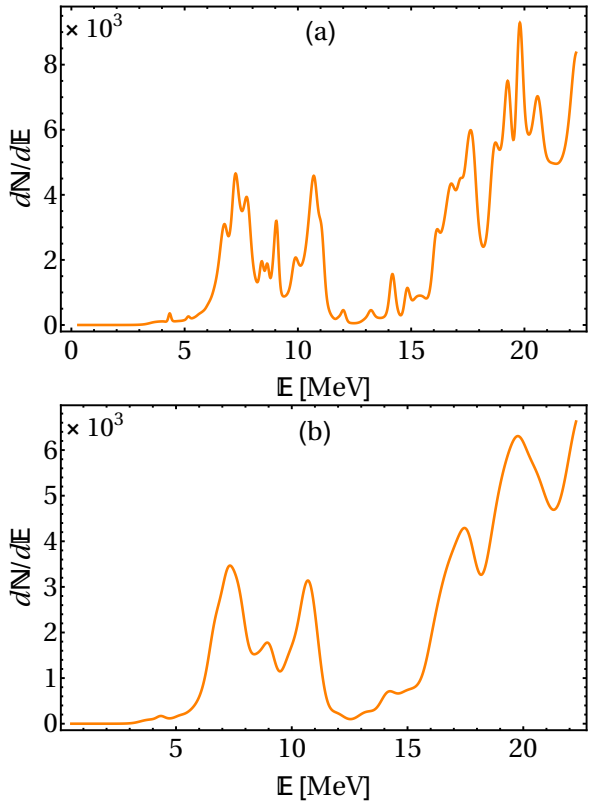

Figure 4. The number of neutron events per laser pulse per unit energy of the incident ^{13}C ions interacting with a plasma target. For the TNSA model, the thickness of the ^{13}C target is 5 μm, the peak intensity of the incident laser is 10^{20} W/cm^2, the peak power of the laser pulse is 10 PW, and the pulse duration is 25 fs, respectively (case A discussed in the text). We consider the ^{4}He plasma density $n_{\rm He}$ 5×10^{20} cm^{-3}, the thickness 20 μm, and the temperatures (a) 100 eV and (b) 1 keV, respectively.

P [PW]	10	10	10	10	5	1
I [W/cm^2]	10^{20}	10^{20}	10^{20}	10^{20}	3×10^{19}	10^{19}
$\tau_{\rm laser}$ [fs]	25	25	25	25	50	250
$d_{\rm t}$ [μm]	10	5	1	0.1	5	5
^{13}C ion charge state	6+	6+	6+	6+	5+	4+
$\mathbb{N}$ for plasma [10^3]	39.3	49.0	60.3	63.0	11.4	5.50
$\mathbb{N}$ for gas target [10^3]	34.6	43.1	53.0	55.5	10.3	5.06

Table 2. The total number $\mathbb{N}$ of neutron events per laser pulse for ^{4}He gas and plasma targets. We consider the target density $n_{\rm He}$ = 5×10^{20} cm^{-3} and target thickness 20 μm for both cases. For the ^{4}He plasma target, the plasma temperature is 100 eV. Results for several laser parameter sets and target thicknesses for TNSA are presented.

plasma and gas targets increases with increasing density of ^{4}He target. As shown in Table 3, the difference reaches $\sim$ 20% for the density $n_{\rm He} = 10^{21}$ cm^{-3}. However, such high density gas jets target are experimentally more challenging to realize.

$n_{\rm He}$ [cm^{-3}]	10^{21}	5×10^{20}	10^{20}
$\mathbb{N}$ for plasma [10^4]	10.3	4.90	0.913
$\mathbb{N}$ for gas target [10^4]	8.62	4.31	0.862

Table 3. The total number $\mathbb{N}$ of neutron events per laser pulse for ^{4}He gas and plasma targets. The thickness of the ^{4}He target is in both cases 20 μm. For the plasmas target, the temperature is 100 eV. In the TNSA part, the thickness of the ^{13}C target is 5 μm, the peak intensity of the incident laser is 10^{20} W/cm^2, the peak power of the laser pulse is 10 PW, and the pulse duration is 25 fs, respectively (case A discussed in the text).

P [PW]	10	5	1	10	5	1
I [W/cm^2]	10^{20}	3×10^{19}	10^{19}	10^{20}	3×10^{19}	10^{19}
$\tau_{\rm laser}$ [fs]	25	50	250	25	50	250
$d_{\rm t}$ [μm]	5	5	5	5	5	5
^{13}C ion charge state	6+	5+	4+	6+	5+	4+
T [keV]	0.5	0.5	0.5	1	1	1
$\mathbb{N}$ for plasma [10^3]	43.7	10.3	5.10	43.5	10.1	5.08
$\mathbb{N}$ for gas target [10^3]	43.1	10.2	5.06	43.1	10.2	5.06

Table 4. The total number $\mathbb{N}$ of neutron events per laser pulse for selected temperatures T of the ^{4}He plasma target, compared also with the case of a gas target. The density of the ^{4}He target is all cases $n_{\rm He} = 5\times10^{20}$ cm^{-3} and its thickness 20 μm, respectively.

We also study the effects of the plasma temperature on the total number of neutron events. The results of the number $\mathbb{N}$ of neutron events per laser pulse for selected temperatures T of ^{4}He plasmas are shown in Table 4. The values show that for the plasma temperatures 500 eV and 1 keV, the differences between the two scenarios of fast ions interacting with the plasma target and the gas target are much smaller than the ones shown in Tables 2 and 3. The screening effects are very small for high plasma temperatures at the densities considered. Furthermore, with increasing plasma temperature, the energy contribution from the plasma to the reaction center-of-mass energy grows. This will also effect the number of neutron events. Therefore, as shown in Table 4, for the case of C^{5+} and $T = 1$ keV, the number of neutron events in the plasma can be even smaller than the one in the gas target.

5. SUMMARY AND CONCLUSIONS

We have investigated theoretically a proposed experimental setup for nuclear reactions in laser-generated plasmas at ELI-NP, where two laser beams generate two colliding plasmas (Roth et al. 2015). One of this two plasmas is a rapidly streaming plasma (ion flow), which is produced by an intense laser pulse interacting on a solid target through the TNSA mechanism. The second plasma in this experimental setup is a cold plasma which is produced by the interaction of a second laser pulse on a gas jet target. We have used an isothermal, fluid model (Mora 2003; Fuchs et al. 2006) to model the TNSA scheme. With the ion spectrum obtained from this model, we have studied the fusion reactions in the interaction of the rapidly streaming plasma (ion flow) on the secondary plasma.

As the first case of study, we have considered the reaction ^{13}C(^{4}He,n)^{16}O, which is one of the important helium burning processes as well as one of the main neutron sources for s-process (De Loore & Doom 1992; Gallino et al. 1998; Heil et al. 2008). We have obtained the neutron spectra and the total numbers of neutron events expected at this experimental setup, based on the ELI-NP laser parameters Roth et al. (2015). We have found that it is possible to determine the plasma screening enhancement factor (Salpeter 1954; Gruzinov & Bahcall 1998) for fusion reactions in plasmas, by detecting the difference of the reaction events between the two scenarios of ion flow interacting with the plasma target and the gas target. By selecting appropriate experimental conditions, this difference of neutron events for reaction ^{13}C(^{4}He,n)^{16}O exceeds 10% and even can reach $\sim$ 20%. The study in this work shows a possible way to access experimentally and to understand the plasma screening effect for nuclear reactions in stellar environments in the weak-screening regime. This could allow for the first time the evaluation of nuclear reactions in stellar environments. While it is obvious that laser-generated plasmas in the laboratory can not cover all parameter ranges present in astrophysical environments, a verification of the screening theory in the available weak-screening regime would be very valuable and significantly advance the field of nuclear astrophysics.

We thank C. H. Keitel and S. Tudisco for fruitful discussions.

REFERENCES

Adelberger, E. G., García, A., Robertson, R. G. H., et al. 2011, Rev. Mod. Phys., 83, 195

Aliotta, M., Raiola, F., Gyürky, G., et al. 2001, Nucl. Phys. A, 690, 790

Assenbaum, H. J., Langanke, K., & Rolfs, C. 1987, Z. Phys. A, 327, 461

Atzeni, S., & Meyer-ter Vehn, J. 2004, The Physics of Inertial Fusion: BeamPlasma Interaction, Hydrodynamics, Hot Dense Matter (Oxford: Oxford University Press)

Bernitt, S., Brown, G. V., Rudolph, J. K., et al. 2012, Nature, 492, 225

De Loore, C. W. H., & Doom, C. 1992, Structure and Evolution of single and binary stars (Springer Science + Business Media)

Dzitko, H., Turck-Chièze, S., Delbourgo-Salvador, P., & Lagrange, C. 1995, The Astrophysical Journal, 447, 428

Engstler, S., Krauss, A., Neldner, K., et al. 1988, Phys. Lett. B, 202, 179

Engstler, S., Raimann, G., Angulo, C., et al. 1992, Z. Phys. A, 342, 471

Fuchs, J., Cowan, T. E., Audebert, P., et al. 2003, Phys. Rev. Lett., 91, 255002

Fuchs, J., Antici, P., d'Humières, E., et al. 2006, Nature physics, 2, 48

Gallino, R., Arlandini, C., Busso, M., et al. 1998, The Astrophysical Journal, 497, 388

Graboske, H. C., Dewitt, H. E., Grossman, A. S., & Cooper, M. S. 1973, The Astrophysical Journal, 181, 457

Greife, U., Gorris, F., Junker, M., Rolfs, C., & Zahnow, D. 1995, Z. Phys. A, 351, 107

Gruzinov, A. V., & Bahcall, J. 1998, The Astrophysical Journal, 504, 996

Harissopulos, S., Becker, H. W., Hammer, J. W., et al. 2005, Phys. Rev. C, 72, 062801

Hegelich, M., Karsch, S., Pretzler, G., et al. 2002, Phys. Rev. Lett., 89, 085002

Heil, M., Detwiler, R., Azuma, R. E., et al. 2008, Phys. Rev. C, 78, 025803

Keller, G. 1953, The Astrophysical Journal, 118, 142

Labaune, C., Baccou, C., Depierreux, S., et al. 2013, Nature communications, 4, 2506

Macchi, A., Borghesi, M., & Passoni, M. 2013, Rev. Mod. Phys., 85, 751

Malka, G., & Miquel, J. L. 1996, Phys. Rev. Lett., 77, 75

Mascali, D., Tudisco, S., Bonanno, A., et al. 2010, Radiation Effects and Defects in Solids, 165, 730

Mora, P. 2003, Phys. Rev. Lett., 90, 185002

Negoita, F., Roth, M., Thirolf, P. G., et al. 2016, Romanian Reports in Physics, 68, Supplement, S37

Oreshkina, N. S., Cavaletto, S. M., Keitel, C. H., & Harman, Z. 2014, Phys. Rev. Lett., 113, 143001

Raiola, F., Migliardi, P., Gyürky, G., et al. 2002, Eur. Phys. J. A, 13, 377
Rolfs, C. 2001, Prog. Part. Nucl. Phys., 46, 23
Rolfs, C., & Somorjai, E. 1995, Nucl. Instrum. Methods Phys. Res., Sect. B, 99, 297
Roth, M., Thirolf, P., Tudisco, S., et al., eds. 2015, Laser driven nuclear physics at ELI-NP – technical design report (ELI-NP)
Salpeter, E. 1954, Australian Journal of Physics, 7, 373
Salpeter, E. E., & Van Horn, H. M. 1969, The Astrophysical Journal, 155, 183
Schmid, K., & Veisz, L. 2012, Rev. Sci. Instrum., 83, 053304
Wilks, S. C., Kruer, W. L., Tabak, M., & Langdon, A. B. 1992, Phys. Rev. Lett., 69, 1383
Xu, Y., Takahashi, K., Goriely, S., et al. 2013, Nucl. Phys. A, 918, 61